Morphodynamic hierarchy and the fabric of the sedimentary record

Vamsi Ganti[1,2], Elizabeth A. Hajek[3], Kate Leary[1], Kyle M. Straub[4], and Chris Paola[5]

[1]Department of Geography, University of California Santa Barbara, Santa Barbara, CA

[2]Department of Earth Science, University of California Santa Barbara, Santa Barbara, CA

[3]Department of Geological Sciences, Pennsylvania State University, State College, PA

[4]Department of Earth and Environmental Sciences, Tulane University, New Orleans, LA

[5]Department of Earth Science and St. Anthony Falls Laboratory, University of Minnesota, Twin-Cities, MN

Contents of this file

Introduction

This supplement contains a further description of:

a. Our numerical methods, with results for different parameter values that support our primary conclusions in the main text (text S1)
b. Details of the experimental configuration and data collection methods of the existing river dune experiments used in our study (text S2)
c. Information about the detrending method used on the field data of river dunes and bars from the Lower Mississippi River (text S3)
d. Details of the delta experiments analyzed here and methods used to evaluate the percentiles of preserved elevations in stratigraphy (text S4)

Text S1. Supplementary information for numerical simulations

We used a two-parameter Gamma distribution to describe the natural variability in the topographic relief within individual hierarchical levels, given by:

$$f(h_i) = \frac{h_i^{\alpha-1} exp(-h_i/\beta)}{\beta^\alpha \Gamma(\alpha)} \qquad (S1)$$

where α is the shape parameter and β is the scale parameter, and h_i denotes the normalized topographic relief of a given hierarchical level, i. Our choice of the distribution is supported by both experimental and field data (Fig. S1; Paola & Borgman, 1991). The Gamma distribution has a positive mode for a shape parameter greater than 1, and we used a fixed value of $\alpha = 5$ in all our simulations because topographic relief within each hierarchical level has a dominant, positive mode in natural systems.

We used a total of four morphodynamic hierarchical levels (with means of 0.25, 1, 3, and 8) that span a vertical scale of 0.1 to 10 times the bankfull flow depth, consistent with natural systems. Conceptually, these hierarchical levels represent in-channel processes (e.g., ripple and dune migration), channel-scale processes (e.g., bar migration), channel-belt-scale processes (e.g., avulsions) and changes driven by allogenic forces (e.g., regradation forced by relative sea-level changes). Previous studies (e.g., Miall, 1985, 2015; Holbrook & Miall, 2020) have discussed several processes that span a multitude of scales in fluvial systems in greater detail than we have here; however, we note that majority of these processes can be classified into the one of the four major hierarchical levels adopted in our study. In addition to the topographic relief, we also characterized the migration timescale of an individual hierarchical level, i, using a uniform random variable with mean T_i. We varied the ratio of migration timescales across hierarchical levels in our simulations.

For a given parameter set, we generated 1000 independent topographic sequences, $\eta_{total}(t)$, where:

$$\eta_{total}(t) = \sum_{i=1}^{N} \eta_i(t) + \sigma t \qquad (S2)$$

where $\eta_i(t)$ is the elevation time series within an individual hierarchical level i, $N \leq 4$ is the total number of hierarchical levels, and σ is the rate of net drift. The vertical distance between the successive maxima and minima of $\eta_i(t)$ was randomly sampled using equation (S1), and the horizontal distance between these points is determined by the migration timescale. Finally, we linearly interpolated the elevations between the successive maxima and minima to yield an individual realization of $\eta_i(t)$. An example realization is shown is Figure 1d of the main text.

In the main text, we showed results of a base case, with $T_2/T_1 = 5$, $T_3/T_1 = 50$, $T_4/T_1 = 100$, and $\sigma = 0$. Here, we report the entire cumulative density functions of $p_{i,N}$ for which we computed the preserved extremality index (Fig. S2). In addition, we varied the evolution timescales of hierarchical levels to $T_2/T_1 = 5$, $T_3/T_1 = 100$, and $T_4/T_1 = 200$, and our results were consistent, i.e., the preservation of the ith level is a function of the relative migration timescales of the immediate higher-order level and the ith level (Fig. S3). Furthermore, the increase in preservation potential of medial topography with decrease in ratio of T_{i+1}/T_i was not limited to $i = 1$ alone. Figure S4 shows results for higher-order hierarchical levels, which produce similar trends as the shortest-wavelength topography, reported in main text (Fig. 2b).

Text S2. Supplementary information on river dune experiments

We analyzed data from two bedform evolution experiments, called the steady-state experiment and the fast flood experiment (Ganti et al., 2013; Martin & Jerolmack, 2013). Both

experiments were conducted in a 15 m long, 0.92 m wide, and 0.65 m deep titling flume at St. Anthony Falls Laboratory, University of Minnesota, with unimodal sediment of median grain size 0.37 mm. In the steady-state experiment, constant water discharge of 0.08 m^3/s was run until the bedforms reached a statistical equilibrium, and data of water and bed surface elevation evolution was collected every 45 s for 20 hr (Ganti et al., 2013). The average bedform height, length, and migration rates during the experiment were 20 mm, 300 mm, and 0.32 mm/s, respectively (Ganti et al., 2013; Leary & Ganti, 2020). We constructed the synthetic stratigraphy for this 6 m long profile, and tracked the original percentile of the preserved elevations from the distribution of elevations present at the given time. For example, if $\eta(x_{pres}, t_{pres})$ denotes the preserved elevation, we tracked the percentile that this elevation represents from the distribution of all possible elevations present at that time, i.e., $\eta(x, t_{pres})$.

In the fast flood experiment, the water discharge was gradually increased from 0.04 m^3/s to 0.115 m^3/s and back down to 0.04 m^3/s (Martin & Jerolmack, 2013). The duration of the waxing and waning flows was 1 hr, and data of water and bed surface elevation evolution were collected for 10 hr at a temporal resolution of 17 s (Martin & Jerolmack, 2013). During the waxing flow, the bedforms grew in height from 25 to 50 mm; however, the bedform decay during waning flow occurred through the cannibalization process, which was slow when compared to the growth process, leading to bedform hysteresis (Martin & Jerolmack, 2013; Leary & Ganti, 2020). During the cannibalization process, the peak-flood-equilibrated bedforms and smaller, superimposed bedforms equilibrated with lower flow conditions co-exist (Fig. S5; Martin & Jerolmack, 2013; Myrow *et al.*, 2018; Leary & Ganti, 2020), i.e., morphodynamic hierarchy is present. The bedform turnover timescale quantifies the time for which the cannibalization process occurs, and consequently the duration for which morphodynamic hierarchy was present during the experiment (Leary & Ganti, 2020). Martin and Jerolmack (2013) estimated this timescale to be 5.4 hr from the time of the peak-flood discharge for the fast-flood experiment.

Similar to the steady-state experiment, we constructed the synthetic stratigraphy for an 8-m long profile from the fast flood experiment and tracked the original percentiles of the preserved elevations. We separately evaluated Ω for the duration for which morphodynamic hierarchy was present and also when morphodynamic hierarchy was absent (Fig. 3d in main text). In addition, we also report the cumulative density functions of the original percentiles of preserved elevations in Figure S6.

Text S3. Supplementary information on field data of the Lower Mississippi River

We analyzed two 40-km long profiles of the Lower Mississippi River, reported by Leclair (2011). We refer the reader to the original publication about the data acquisition methods and the location of the long profile. We constructed the synthetic stratigraphy from these two profiles, and tracked the elevations of the earlier-time profile that were preserved. For consistency with our model, we removed the trend imposed by the bars on the dune topography using a piecewise linear function (Fig. S7). We evaluated Ω for the detrended, dune topography (Fig. 3d in main text). Figure S6 also shows the cumulative density function of the original percentiles of the preserved elevation for the Lower Mississippi data.

Text S4. Supplementary information on delta experiments

We compared the nature of stratigraphic preservation in two delta experiments. First, we analyzed a delta experiment conducted in the river-ocean facility at the Caltech Earth-surface Dynamics Laboratory. The experimental setup consisted of a 7 m long, 7 cm wide channel that drained into a 5 m by 3 m delta basin. We analyzed the variable discharge experiment (Ganti et al., 2016a), which was conducted with subcritical flows

and constant base level, where the water discharge was varied between low (duration of 40 mins) and high flows (duration of 15 mins) for a total ~150 hrs. We term this the cohesionless experiment, which was conducted using crushed walnut shells of uniform grain size 0.7 mm. The sediment supply was commensurate with water discharge such that the experimental channel transported sediment at capacity within the normal flow reach. High-resolution data (grid resolution of 3 mm by 3 mm, and vertical resolution of 0.1 mm) of bed surface evolution was collected at the end of each flow after the flow was switched off. We used a time series of topographic evolution for a 600 mm long profile that was perpendicular to the longitudinal direction of the flume, which was 90 cm downstream of the change in confinement of the flume. A total of 41 avulsions occurred during the experiment, and the strike-oriented section we analyzed here was downstream of the avulsion sites. Avulsions were driven by persistent backwater hydrodynamics and progradation caused delta-top aggradation, and there was no systematic trend in cross-stream topography. The average avulsion timescale for the entire experiment was 3.45 ± 0.55 hr (Ganti et al., 2016b). We refer the reader to the original publications for a detailed description of the experimental methods and deltaic evolution and stratigraphy (Ganti et al., 2016a; b, 2019).

We contrasted the cohesionless experiment with an experiment conducted in the Tulane Delta Basin with cohesive sediment, constant base-level rise of 0.25 mm/hr, and constant sediment and water discharge (Straub et al., 2015). We term this the cohesive experiment. Sediment cohesion was achieved through the addition of a polymer, modeled after a previous study (Hoyal & Sheets, 2009), and the median grain size of sediment was 67 μm. The maximum channel depth in the experiment was ~12.2 mm, which yields a compensational timescale of 48.8 hr (Wang et al., 2011). Avulsion timescales were not directly measured; however, previous studies indicate that the compensational timescale is often an order-of-magnitude higher than lobe-scale avulsion timescale (Wang et al., 2011). This suggests that both the cohesionless and cohesive experiments had a similar avulsion timescale; however, they significantly differed in the channel-migration timescales because of differences in sediment cohesive strength.

We analyzed one strike-oriented section from the cohesive delta experiment. Bed elevation data were collected at a horizontal spacing of 5 mm and a temporal resolution of 1 hr. We refer the reader to the original publications for further details about the experimental facility and data collection methods (Straub et al., 2015; Li et al., 2016, 2017). Unlike the cohesionless experiment, the cohesive experiment had both a long-term temporal trend in elevation data because of constant sea-level rise, and the delta surface had a cross-stream topographic trend. Therefore, for the cohesive experiment, we removed the long-term temporal trend in topographic data and the spatial non-stationarity in cross-stream topography, following Straub and Wang (2013). We then evaluated the percentiles of preserved elevations in this detrended space, which is equivalent to evaluating the percentiles of the preserved elevations relative to their theoretical graded-profile.

Figure 4e in the main text shows the preserved extremality index for both these experiments, and Figure S8 shows the cumulative density functions of the original percentiles of the preserved elevations.
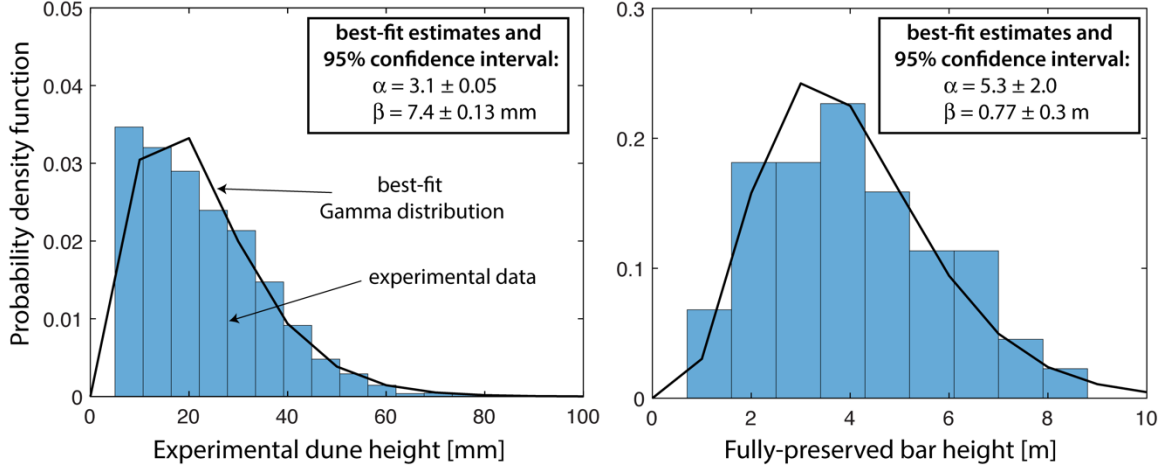
Figure S1. Probability distribution functions of river dune (left panel) and bar heights (right panel). The measured densities are shown as blue bars and the black line is the best-fitting two-parameter Gamma distribution. The experimental dune heights ($n = 30{,}692$) are from the steady-state experiment (Ganti et al., 2013). The fully-preserved bar heights ($n = 49$) are measured from the Lower Castlegate Sandstone (Hajek, 2005; Hajek & Heller, 2012).
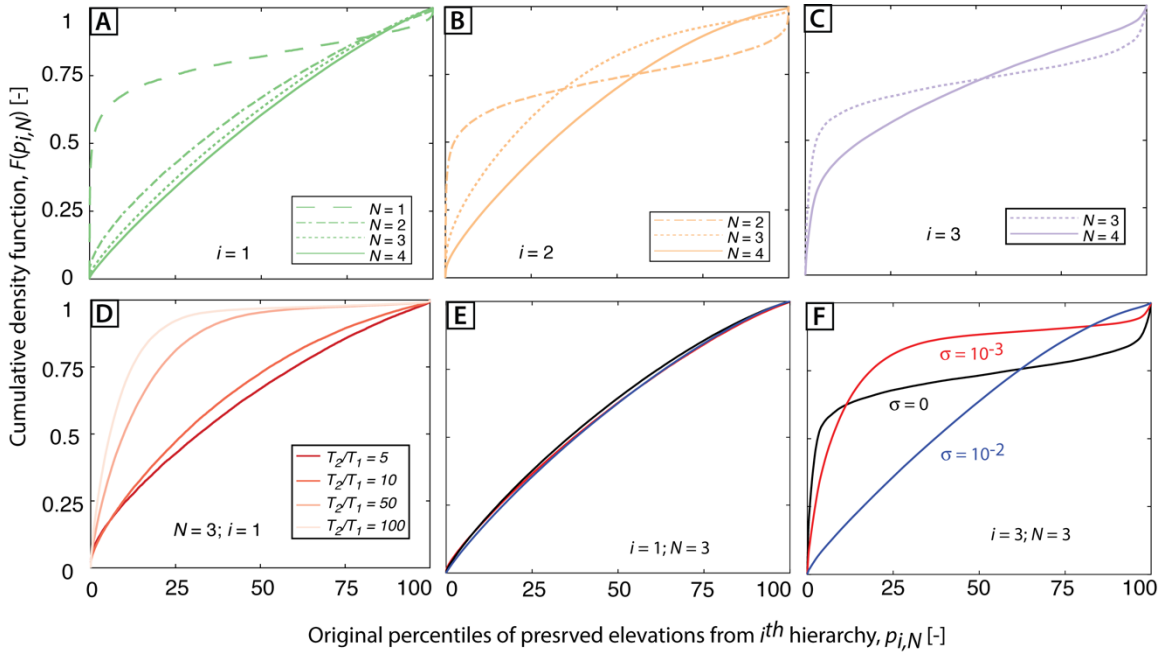
Figure S2. Original percentiles of preserved elevations from individual hierarchies ($i =$ (a) 1, (b) 2, (c) 3) for different values of total morphodynamic hierarchies (N). (d) Original percentiles of preserved elevations of the shortest-wavelength topography when $N = 3$, with varying ratios of T_2/T_1. Percentiles of preserved elevations of the (e) shortest- and (f) longest-wavelength topography for differing values of net drift rate, denoted as σ. Figure 2 in the main text shows the preserved extremality index evaluated using these cumulative density functions.
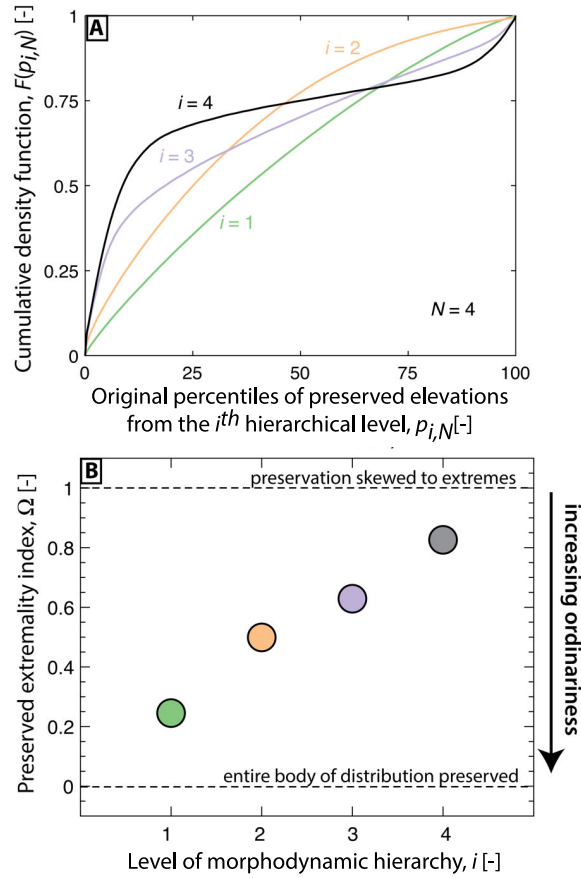
Figure S3. (a) Original percentiles of preserved elevations from the shortest to longest-wavelength topography in the presence of $N = 4$ hierarchical levels. These simulations were performed with $T_2/T_1 = 5$, $T_3/T_1 = 100$, and $T_4/T_1 = 200$, and results are from 1000 independent realizations with same parameter values. (b) Preserved extremality index as a function of the hierarchy level, i. Relative migration timescales of hierarchical levels were different than reported in the main text. Our results are consistent in that preservation of ordinary elevations is enhanced at all hierarchical levels except the highest level, i.e., $i = N$.
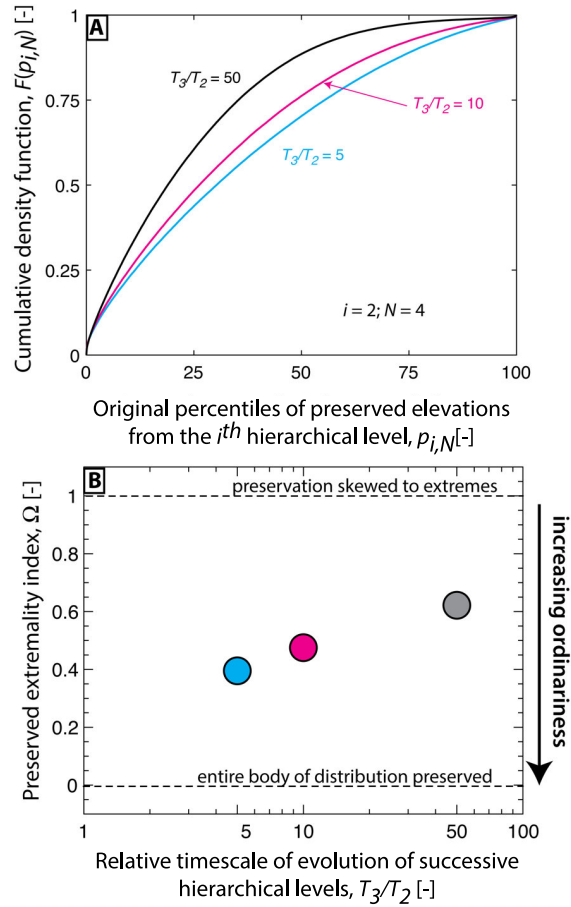
Figure S4. (a) Original percentiles of preserved elevations and (b) the preserved extremality index of the 2nd morphodynamic hierarchical level for different values of T_3/T_2. Results are similar to those reported in the main text (Fig. 2b), where comparable values of T_3 and T_2 cause enhanced preservation of ordinary topography from the 2nd hierarchical level, whereas disparate values of T_3 and T_2 skews the preservation of 2nd hierarchical level towards extreme topographic elements. Results are from an ensemble of 1000 independent realizations for each parameter set.
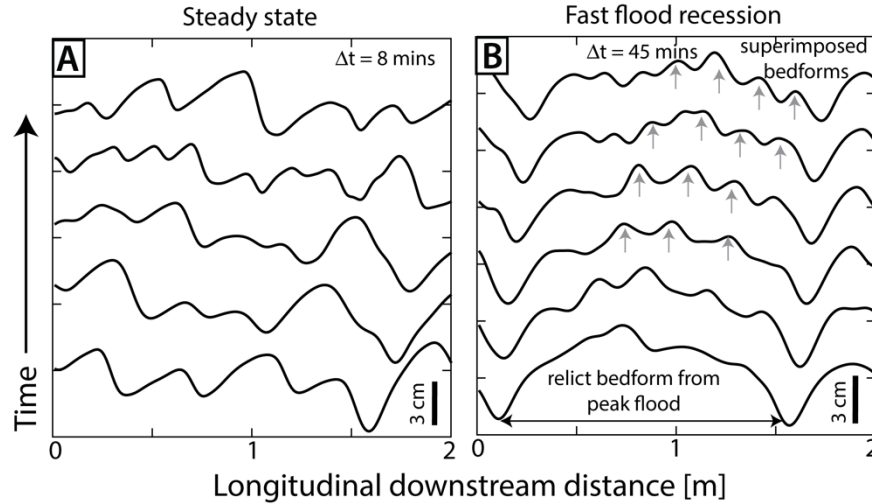
Figure S5. Comparative plots of the time evolution of a 2-m longitudinal bedform profiles in the (a) steady-state and (b) unsteady experiment. The profiles are vertically offset, and each profile is 8 and 45 mins apart in the steady and unsteady experiment, respectively. The bedform profiles in the unsteady experiment are from the flood recession where the morphodynamic hierarchy is apparent. The gray arrows indicate the smaller, superimposed dunes that eventually cannibalize the peak-flood-equilibrated bedforms. In contrast, there is no apparent morphodynamic hierarchy in the steady-state bedforms.
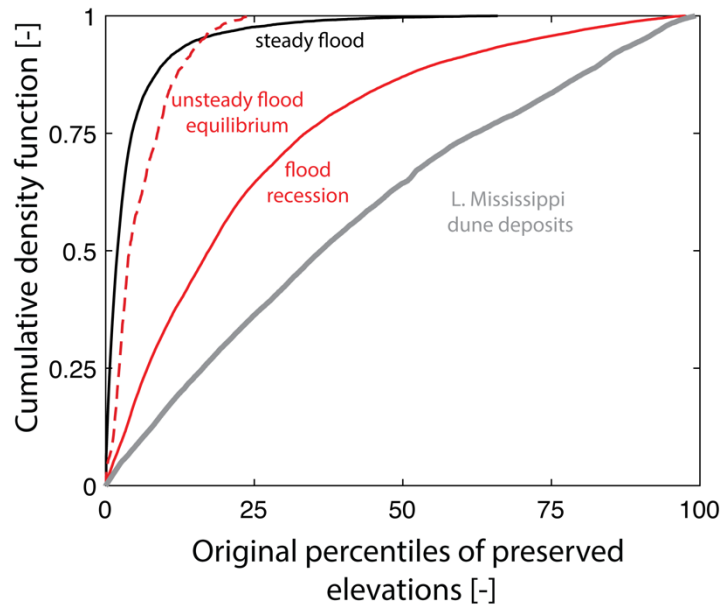
Figure S6. Cumulative density functions of the original percentiles of preserved dune elevations in the steady-state experiment (black line), unsteady experiment during the presence (red, solid line) and absence of morphodynamic hierarchy (red, dashed line), and the Lower Mississippi River (gray line).
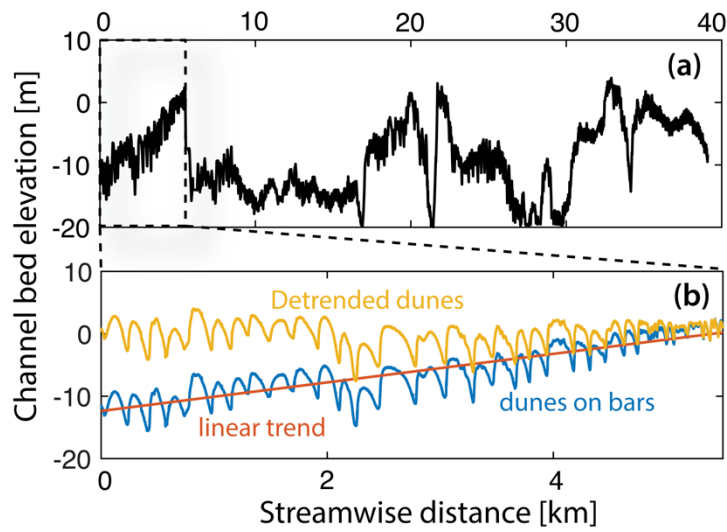
Figure S7. (a) The earlier time 40-km long profile of Lower Mississippi River (Leclair, 2011). (b) The blue profile shows a close-up of the first 5-km stretch of the long profile along with the linear trend imposed by bar topography (red line). We removed this linear trend from the dune topography to evaluate the original percentiles of preserved elevations, similar to our numerical simulations.
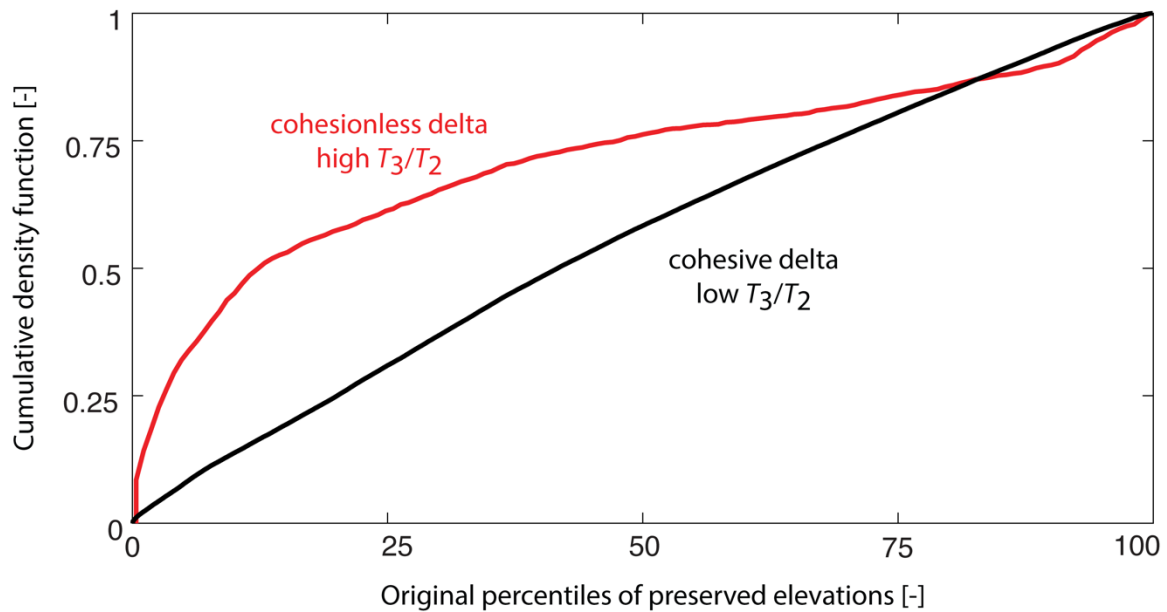
Figure S8. Cumulative density functions of the original percentiles of preserved elevations for the cohesionless (red line) and cohesive experiments (black line).

Supplementary references

Ganti, V., Chadwick, A.J., Hassenruck-Gudipati, H.J., Fuller, B.M. and Lamb, M.P. (2016a) Experimental river delta size set by multiple floods and backwater hydrodynamics. Sci Adv. doi: 10.1126/sciadv.1501768

Ganti, V., Chadwick, A.J., Hassenruck-Gudipati, H.J. and Lamb, M.P. (2016b) Avulsion cycles and their stratigraphic signature on an experimental backwater-controlled delta. *J. Geophys. Res. Earth Surf.*, 121, 1651–1675.

Ganti, V., Lamb, M.P. and Chadwick, A.J. (2019) Autogenic Erosional Surfaces in Fluvio-deltaic Stratigraphy from Floods, Avulsions, and Backwater Hydrodynamics. *J. Sediment. Res.*, 89, 815–832.

Ganti, V., Paola, C., Foufoula-Georgiou, E. and Foufoula Georgiou, E. (2013) Kinematic controls on the geometry of the preserved cross sets. *J. Geophys. Res. Earth Surf.*, 118, 1296–1307.

Hajek, E.A. (2005) Analysis of alluvial architecture in the lower Castlegate Sandstone (Campanian, Helper, Utah) using LIDAR imaging.

Hajek, E.A. and Heller, P.L. (2012) Flow-Depth Scaling In Alluvial Architecture and Nonmarine Sequence Stratigraphy: Example from the Castlegate Sandstone, Central Utah, U.S.A. *J. Sediment. Res.*, 82, 121–130.

Holbrook, J. and Miall, A.D. (2020) Time in the Rock: A field guide to interpreting past events and processes from a fragmentary siliciclastic archive. *Earth-Science Rev.*, 103121.

Hoyal, D.C.J.D. and Sheets, B.A. (2009) Morphodynamic evolution of experimental cohesive deltas. J Geophys Res Earth Surf. doi: 10.1029/2007JF000882

Leary, K.C.P. and Ganti, V. (2020) Preserved Fluvial Cross Strata Record Bedform Disequilibrium Dynamics. *Geophys. Res. Lett.*, 47, e2019GL085910.

Leclair, S.F. (2011) Interpreting fluvial hydromorphology from the rock record: Large-river peak flows leave no clear signature. *From river to rock Rec. Preserv. Fluv. sediments their Subseq. Interpret. SEPM Spec. Publ.*, 97, 113–123.

Li, Q., Matthew Benson, W., Harlan, M., Robichaux, P., Sha, X., Xu, K. and Straub, K.M. (2017) Influence of Sediment Cohesion on Deltaic Morphodynamics and Stratigraphy Over Basin-Filling Time Scales. *J. Geophys. Res. Earth Surf.*, 122, 1808–1826.

Li, Q., Yu, L. and Straub, K.M. (2016) Storage thresholds for relative sea-level signals in the stratigraphic record. *Geology*, 44, 179–182.

Martin, R.L. and Jerolmack, D.J. (2013) Origin of hysteresis in bed form response to unsteady flows. *Water Resour. Res.*, 49, 1314–1333.

Miall, A. (1985) Architectural-Element Analysis : A New Method of Facies Analysis Applied to Fluvial Deposits. *Earth-Science Rev.*, 22, 261–308.

Miall, A.D. (2015) Updating uniformitarianism: stratigraphy as just a set of 'frozen accidents.' *Geol. Soc. London, Spec. Publ.*, 404, 11–36.

Myrow, P.M., Jerolmack, D.J. and Perron, J.T. (2018) Bedform Disequilibrium. *J. Sediment. Res.*, 88, 1096–1113.

Paola, C. and Borgman, L. (1991) Reconstructing random topography from preserved stratification. *Sedimentology*, 38, 553–565.

Straub, K.M., Li, Q. and Benson, W.M. (2015) Influence of sediment cohesion on deltaic shoreline dynamics and bulk sediment retention: A laboratory study. *Geophys. Res. Lett.*, 42, 9808–9815.

Straub, K.M. and Wang, Y. (2013) Influence of water and sediment supply on the long-term evolution of alluvial fans and deltas: Statistical characterization of basin-filling sedimentation patterns. *J. Geophys. Res. Earth Surf.*, 118, 1602–1616.

Wang, Y., Straub, K.M. and Hajek, E.A. (2011) Scale-dependent compensational stacking: An estimate of autogenic time scales in channelized sedimentary deposits. *Geology*, 39, 811–

814.